Journal of Hazardous Materials 400 (2020) 123139

Contents lists available at ScienceDirect

Journal of Hazardous Materials

journal homepage: www.elsevier.com/locate/jhazmat

Immobilizing magnetite onto quartz sand for chromium remediation

Julian Sorwat[a], Adrian Mellage[b], Andreas Kappler[a], James M. Byrne[a,c,*]

[a] Geomicrobiology, Center for Applied Geosciences, University of Tübingen, Tübingen 72074, Germany
[b] Hydrogeology, Center for Applied Geosciences, University of Tübingen, Tübingen 72074, Germany
[c] School of Earth Sciences, University of Bristol, Queens Road, Bristol, BS8 1QU, UK

GRAPHICAL ABSTRACT

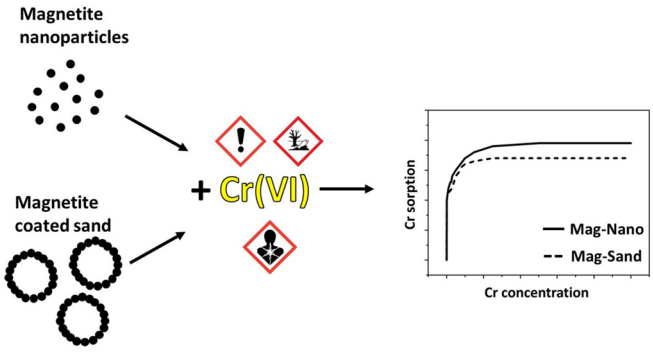

ARTICLE INFO

Editor: Navid B Saleh.

Keywords:
Nanoparticles
Coating
Abiogenic
Biogenic
Sorption

ABSTRACT

Magnetite nanoparticles are often promoted as remediation agents for heavy metals such as chromium due to their reactivity and high surface area. However, their small size also makes them highly mobile increasing the risk that reacted pollutants will be transported to different locations rather than being safely controlled. Released to aquatic environments, aggregation leads to a loss of their nano-specific properties and contaminant-removal capacity. We immobilized magnetite onto sand to overcome these issues whilst maintaining reactivity. We compare biogenic magnetite and abiogenic magnetite coated sand against magnetite nanoparticles. Magnetite coatings mostly exhibited a Fe(II)/Fe(III) ratio close to stoichiometry (0.5). We tested the efficacy of the magnetite-coated sand to adsorb chromium, with respect to biogenic/abiogenic nanoparticles. Langmuir-type sorption of Cr(VI) onto magnetite (4.32 mM total Fe) was observed over the tested concentration range (10–1000 µM). Biogenic nanoparticles showed the highest potential for Cr(VI) removal with maximum adsorption capacity (Q_{max}) of 1250 µmol Cr/g Fe followed by abiogenic nanoparticles with 693 µmol Cr/g Fe. All magnetite coated sands exhibited similar sorption behavior with average Q_{max} ranging between 257 − 471 µmol Cr/g Fe. These results indicate coating magnetite onto sand may be more suitable than free nanoparticles for treating environmental pollutants such as chromium.

1. Introduction

Declining water quality has become an issue of global concern as human populations grow, industrial and agricultural activities expand, and climate change threatens to cause major alterations to the hydrological cycle and human life. This is especially true in cases where

* Corresponding author at: Geomicrobiology, Center for Applied Geosciences, University of Tübingen, Tübingen 72074, Germany.
E-mail address: james.byrne@bristol.ac.uk (J.M. Byrne).

https://doi.org/10.1016/j.jhazmat.2020.123139
Received 7 February 2020; Received in revised form 2 June 2020; Accepted 4 June 2020
Available online 11 June 2020

pollutants are present in areas close to drinking water supplies, with environmental contaminants posing serious risks to living organisms and human health (Brezonik and Arnold, 2012). The type of pollution varies from region to region, including organic compounds, pathogens, metalloids such as antimony or arsenic, and heavy metals such as vanadium (Duruibe et al., 2007). One pollutant which is gaining increasing attention is chromium (Cr) due to its presence in trace concentrations in drinking water (Harijan and Chandra, 2016; World Health Organization, 1996) (e.g. North America (Meranger et al., 1979; US Environmental Protection Agency, 1987)) and its ongoing release into the environment as a result of industrial processes such as plating, alloying, tanning, inhibition of water corrosion, textile dyes, pigments, ceramic glazes, pressure-treated lumber and refractory bricks (Avudainayagam et al., 2003). World Health Organization (WHO) guidelines recommend a maximum safe drinking water level concentration of 50 μg/L total Cr, although the German Environmental Agency (UBA) has discussed lowering the limit to 0.3 μg/L, within Germany, while US-EPA regulations are currently also under revision (Environmental Protection Agency, 2019; World Health Organization, 2017; Umweltbundesamt, 2012).

The oxidation state of chromium ranges from Cr(−II)–Cr(+VI) with trivalent Cr(III) and hexavalent Cr(VI) being the two most stable oxidation states in the environment. Cr(VI) is a strong oxidant which is toxic to plants, animals, humans and is known to be carcinogenic (Barnhart, 1997). Cr(VI) salts are more soluble than Cr(III) and are highly mobile in the environment. In contrast, Cr(III) has a relatively low solubility and could therefore adsorb strongly to the surface of soil minerals which limits its biological uptake and is considered less toxic than its hexavalent counterpart (Nriagu and Nieboer, 1988).

Several different strategies currently exist for removing chromium from drinking water such as membrane filtration (Yao et al., 2015), ion exchange (Ali et al., 2015), biological remediation (Micera and Dessì, 1988; Peterson, 1975; Salunkhe et al., 1998; Terry and Banuelos, 1999) or adsorption to synthetic Fe(III) oxyhydroxides minerals such as akaganéite or ferrihydrite (Kleinert et al., 2011). Alternatively, adsorption of Cr to magnetite (Fe_3O_4) has been extensively investigated in the literature (Crean et al., 2012; Cutting et al., 2010). Magnetite is a magnetic, mixed-valent iron oxide, i.e. contains both Fe(II) and Fe(III). The Fe(II) present in magnetite can induce a chemisorption reaction which involves the reduction of highly toxic, soluble Cr(VI) and the incorporation of the less toxic Cr(III) into the octahedral sites of the magnetite structure (Cutting et al., 2010; Fendorf and Li, 1996; Ren et al., 2017). Additionally, a further improvement of the magnetite could be achieved by enhancing the stoichiometry through the use of either Fe(III)-reducing or Fe(II)-oxidizing bacteria as recently shown by Sundman et al. (2020). Thus, magnetite has several potential advantages over other iron minerals because it can not only sorb and sequester toxic heavy metals, but unlike ferrihydrite and goethite, the Fe(II) content in magnetite means that it can reduce the oxidation state to less toxic states. Consequently, the efficiency of magnetite as a material for Cr removal can be improved by either increasing the Fe(II) content, or increasing its surface area to volume ratio.

Magnetite nanoparticles, which have an extremely high specific surface area (SSA), can be formed either abiogenically (e.g., by natural weathering or chemical precipitation (Pearce et al., 2012)) or by microbiological processes such as during the microbial reduction of short range ordered Fe(III) (oxyhydr)oxide minerals (Lovley and Phillips, 1986). The method through which magnetite is formed influences particle size, SSA and the Fe(II)/Fe(III) ratio, all of which affect the contaminant removal efficiency (Crean et al., 2012).

The idea of using magnetite nanoparticles to treat Cr is not new (Crean et al., 2012; Ren et al., 2017; Sundman et al., 2020), however, there are many challenges which have yet to be overcome. For instance, nanoparticles, used for in situ remediation, are released to the environment to remove contaminants (Limbach et al., 2008). Upon their release, their mobility and effective surface area can decrease through aggregation leading to a loss of their nano-specific properties and contaminant-removal capacity (Petosa et al., 2010; Phenrat et al., 2009; Tratnyek and Johnson, 2006). Furthermore, nanoparticles released to the environment can present a toxicity hazard. Nanoparticles can penetrate epithelial cells (Berry et al., 2004; Maher et al., 2016; Panyam and Labhasetwar, 2003) and iron-based nanoparticles can also produce reactive oxygen species (ROS) which can cause oxidative injury to cells (Brown et al., 2001; LeBel et al., 1992; Li et al., 2009). A study by García et al. (2011) showed extreme sensitivity of *Daphnia magna* to iron oxides and even found black aggregates, purported to be magnetite, inside the bodies of dead animals.

In addition, the use of magnetic nanoparticles for remediation can have other disadvantages such as the need to use electromagnetic fields for separation from solution or can cause a drop in potential pressure in fixed-bed adsorber columns (Kango and Kumar, 2016; Verbinnen et al., 2013; Chahbani and Tondeur, 2001). If nanoparticles are used, a pressure drop along the column can lead to errors with the estimation of breakthrough time at molar flow rates due to a second order dependence of pressure drop on the particle size. A supporting matrix for magnetite nanoparticles such as inexpensive sand particles, thus, can potentially overcome these transport, agglomeration, pressure and separation issues. The main challenge lies in maintaining the performance of nanoparticles towards Cr removal, while curtailing the potential disadvantages associated with their application.

The main objective of this study was to coat biogenic and abiogenic magnetite onto quartz sand grains, and compare their performance towards Cr(VI) sorption/removal against suspensions of “free” biogenic and abiogenic magnetite nanoparticles. All materials were characterized in terms of the total amount of iron per gram of sand or total iron per liter of solution (for nanoparticles), Fe(II)/Fe(III) ratio, specific surface area (SSA), coating efficiency and maximum sorption capacity towards Cr.

2. Material & methods

2.1. Magnetite synthesis

2.1.1. Sand treatment

Both fine-grained (Ø: 0.1 − 0.5 mm; OPC O. Priess & Co. (GmbH & Co.) KG, Germany) and coarse-grained (Ø: 0.4 − 0.8 mm; Carl Roth GmbH + Co. KG, Germany) sands were acid-washed, in a 1 M HCl bath, overnight. Subsequently, the sands were washed with Milli-Q water (Resistivity: 0.054 μS, Merck™ Milli-Q™, Q-Gard® 2 Purification Cartridge) and dried at 60 °C. The coarse sand was additionally treated in Aqua regia for 5 min to improve the Fe coating efficiency (Kango and Kumar, 2016). This additional step was tested for both pure sands, but an improvement in terms of Fe/g_{sand} by this treatment could only be detected for the coarse sand. Afterwards all sands were washed with Milli-Q water and dried at 60 °C.

2.1.2. Biogenic magnetite nanoparticles and biogenic magnetite sand coating

Fe(III) oxyhydroxide 2-line ferrihydrite was synthesized by precipitation from a $Fe(NO_3)_3{\cdot}9H_2O$ solution by adding 1 M KOH. KOH was added dropwise until a pH of 7.3 was reached. The solution was left without stirring for two hours followed by readjustment to pH 7.5, followed by repeated washing steps by centrifugation in Milli-Q water.

Fine or coarse sand were coated with Fe(III) oxyhydroxide 2-line ferrihydrite (FH-Fine, FH-Coarse) by precipitating the ferrihydrite in the presence of the sand. In this case the $Fe(NO_3)_3{\cdot}9H_2O$ was added to 300 g of sand and stirred manually by hand as KOH was added dropwise. The solution was left overnight on a rolling shaker (15 rpm), washed with Milli-Q water and dried at 40 °C. (Note: drying of the iron-mineral coated sand was done at a lower temperature to avoid temperature induced modifications to the precipitate).

Biogenic magnetite was produced by microbial Fe(III) reduction of

ferrihydrite. *Geobacter sulfurreducens* was cultivated under anoxic conditions (Headspace: N_2/CO_2 v/v; 90/10) at pH 7 in the dark at 30 °C in 250 ml serum bottles containing a mineral medium (Byrne et al., 2015), 30 mM $NaHCO_3$ buffer, 40 mM fumarate as electron acceptor, 25 mM acetate as electron donor and 2 mM cysteine. Growth of the culture was monitored by optical density measurements at 600 nm (OD_{600}). Stationary phase cultures of *G. sulfurreducens* were harvested by centrifugation at 5000 rpm at 10 °C three times for 20 min and washed with bicarbonate buffer (30 mM, pH 7) to prepare a cell suspension with a final cell density of 10^9 cells/mL.

The microbial reduction of ferrihydrite to magnetite was performed under anoxic conditions in 250 ml serum bottles containing 100 ml of a 30 mM $NaHCO_3$ buffer solution (pH 7), 50 mM Fe(III) as ferrihydrite or ferrihydrite-coated sand and 20 mM acetate. The cell suspension of *G. sulfurreducens* was added into the bottles, equivalent to 250 % (v/v) inoculum and incubated in the dark at 30 °C for 24 h. Such a high density of bacteria was added to ensure complete transformation to magnetite and promote the formation of nanoparticles (Byrne et al., 2011). The biogenic magnetite nanoparticles (Bio-NP) or biogenic magnetite-coated fine/coarse sand (Bio-Fine, Bio-Coarse) were then washed three times with anoxic Milli-Q water in an anaerobic chamber (MBraun, 100 % N_2).

2.1.3. Abiogenic magnetite nanoparticles and abiogenic magnetite coated on sand

Abiotic magnetite nanoparticles (Abio-NP) were prepared by precipitation from a solution containing both $FeCl_2$ (1 M) and $FeCl_3$ (2 M) in HCl (0.3 M) by anoxic NH_4OH (20 %) which was added dropwise under continuous stirring at 800 rpm in an anoxic glovebox (100 % N_2). This process leads to the instantaneous precipitation of magnetite nanoparticles. Afterwards the mineral suspension was washed twice in Milli-Q water to remove chloride ions. Abiogenic magnetite coated on coarse/fine sand (Abio-Fine, Abio-Coarse) was synthesized by the addition of a $FeCl_2$ (1 M)/ $FeCl_3$ (2 M) in HCl (0.3 M) solution to 300 g coarse or fine sand. This mixture was stirred manually by hand during the dropwise addition of NH_4OH (20 %) in the glovebox. After the precipitation of magnetite indicated by a color change to black, the sand-Fe mixture was left overnight on a rolling shaker (15 rpm) and then washed with Milli-Q water to remove residual ions. The entire procedure was performed in an anoxic glovebox (100 % N_2).

2.2. Sand and magnetite characterization

2.2.1. Grain size distribution

The grain size distribution of the initial pure fine sand was determined with the Mastersizer 2000 equipped with the wet dispersion unit Hydro 2000S (Malvern Instruments). Data were analyzed with the internal Malvern software (Version 5.61). The initial pure coarse sand was ordered with a specific grain size.

2.2.2. Total iron and iron(II) analysis

Fe(II) and Fe(tot) concentrations of magnetite or precursor material (FH-Fine, FH-Coarse, Pure-Fine and Pure-Coarse sand) were measured by chemical dissolution followed by spectrophotometric ferrozine assay (Stookey, 1970) in triplicate. The different magnetite materials were dissolved in 6 M HCl over 24 h at room temperature in an anoxic glovebox (MBraun; 100 % N_2) followed by a dilution with 1 M HCl to reach the calibration range of the ferrozine standards. Fe(III) concentrations were determined by subtraction of Fe(II) from the Fe(tot) concentration. Spectrophotometric measurements were performed with the monochromator-based UV/VIS spectrophotometer Multiskan GO (Thermo Fisher Scientific) and processed with the SkanIt software 3.2.

2.2.3. Specific surface area determination

The specific surface area (SSA) of the different magnetite materials were quantified with the Micromeritics Gemini VII surface area and porosity analyzer (Micromeritics Instrument Corporation, USA) operating with N_2 as the adsorbate. The instrument was equipped with the VacPrep 061 for sample preparation and was operated with the Gemini VII software (Version 5.01).

2.2.4. Iron coating visualization and quantification of the layer thickness

The success of the sand coating procedure was investigated by visual inspection of the coating with a Leica Z16 APO with a magnification of 2.5× or 9.2× and processed with the Image-Pro Plus software (Version 6.0.0.260, Media Cybernetics). To quantify the layer thickness of the different sand coatings several coated or pure sand grains were embedded in Araldite 2020 epoxy resin and polished. Images were recorded with the Leica DMRX optical microscope. The thickness of the iron coating was determined using the Leica Application Suite (Version 4.60) and ImageJ 1.52p Fiji (Wayne Rasband, National Institute of Health, USA) software. Micrographs were collected at different magnifications (20×, 50×, 100×).

2.3. Sorption experiments

2.3.1. Removal of Cr from solution by magnetite nanoparticles and magnetite-coated sand

Cr(VI) removal by the different types of magnetite was quantified with 24 -h incubation batch-sorption experiments at circumneutral pH (~7) at room temperature over a range of Cr concentrations. The goal of the batch experiment was to determine the ability and capacity of the different types of magnetite to adsorb dissolved Cr. A total volume of 4 ml bicarbonate buffer (22 mM) with an iron concentration of 4.32 mM Fe per vial was used for the sorption experiments. Potassium chromate (K_2CrO_4; Cr(VI)) was added to the vials, with expected concentration of either 10, 50, 75, 100, 150, 250, 500 or 1000 µM Cr(VI). As control groups pure fine/coarse sand were prepared. For the pure sands, the same mass of sand as for the biogenic magnetite coated sand experiments was used. Each setup was prepared in triplicate in the glovebox and kept in the dark on a rolling shaker until sampling. Aqueous and sorbed Cr concentrations were measured after the 24 -h incubation period. For the determination of dissolved Cr concentrations, 1.9 ml of solution were removed and transferred into 2 ml Eppendorf tubes. The samples were centrifuged at 13,400 rpm for 5 min, then 1.8 ml were transferred into an additional 2 ml Eppendorf tube and acidified with 18 µL 65 % HNO_3. Samples were diluted 1:5 and acidified with 2 % HNO_3 to a total volume of 5 mL. The total Cr concentration in the 2 % HNO_3 acidified samples was determined by microwave plasma-atomic emission spectrometer (Agilent 4200 MP-AES, Agilent Technologies, equipped with the Agilent SPS 3 autosampler) measurements at a wavelength of 425.433 nm. Data were processed with the internal Agilent MP Expert software (Version 1.5.0.6545).

A Langmuir isotherm, shown in the Eq. (1), was fitted to the results for each incubation:

$$c_{s,i} = Q_{max,i}\frac{c_{w,i}}{K_{ads,i} + c_{w,i}} \quad (1)$$

where, c_s is the total sorbed Cr concentration, c_w is the Cr concentration left in solution, K_{ads} is the half-saturation concentration, related to the adsorption affinity of Cr to the adsorbent, and Q_{max} is the maximum sorption capacity (the subscript *i* denotes the different adsorbent material). The Q_{max} and K_{ads} were fitted using a nonlinear least-squares solver (*lsqnonlin*) in MATLAB. Parameter uncertainties were estimated via a linearized uncertainty analysis on the log-transformed parameters.

3. Results & discussion

3.1. Mineral synthesis

Results for the characterization of the properties and reactivity of the magnetite-containing materials, pure sand, pure magnetite

Table 1
Characterization of synthesized magnetite nanoparticles (Bio-NP, Abio-NP), magnetite coatings on coarse or fine sand (Bio-Coarse sand, Bio-Fine sand, Abio-Coarse sand and Abio-Fine sand) and the different starting materials (FH-Coarse sand, FH-Fine sand, Pure-Coarse or Pure-Fine sand). Iron total (Fe(tot)) and Fe(II)/Fe(III) were determined via the ferrozine assay. The specific surface area (SSA) was determined by BET measurements. [1]: Ø: 0.4 – 0.8 mm; [2]: Ø: 0.1 – 0.5 mm.

Material	Fe(tot) [mM Fe]	Fe(tot) [mmol Fe/g_{sand}]	Fe(II)/ Fe(III)	SSA [m^2/g]	Attracted to bar magnet
Bio-NP	33.21	–	0.63	37.21	+
Abio-NP	340.00	–	0.53	71.34	+
Bio-Coarse sand	–	0.06	0.48	0.47	+
Bio-Fine sand	–	0.19	0.28	1.64	+
Abio-Coarse sand	–	0.07	0.49	0.67	+
Abio-Fine sand	–	0.10	0.49	1.12	+
FH-Coarse sand	–	0.10	–	1.48	–
FH-Fine sand	–	0.22	–	5.87	–
Pure-Coarse sand[1]	–	–	–	0.07	–
Pure-Fine sand[2]	–	–	–	0.17	–

(abiogenic and biogenic), and magnetite-coated sand are presented in Table 1. The total iron content of the nanoparticles varied by over an order of magnitude between biogenic and abiogenic synthesis method, with Abio-NPs containing 10-fold more Fe. The highest Fe(II)/Fe(III) ratio as well as the highest surface area was measured for the "free" nanoparticles, abiogenic and biogenic (Abio-NP and Bio-NP, respectively). Bio-NPs exhibited the highest Fe(II)/Fe(III) ratio of all samples (0.63) which is higher than the stoichiometric ratio of 0.5 and is likely related to the mode of biogenic magnetite synthesis. During biogenic production Fe(III)-reducing bacteria release Fe(II) into solution, the free Fe(II) then adsorbs onto the FH surface and, via a solid-state conversion, becomes magnetite (Piepenbrock et al., 2011). Conversely, Abio-NPs exhibited a Fe(II)/Fe(III) ratio close to stoichiometric magnetite (0.5). The higher SSA for Abio-NP, compared to Bio-NP, suggests that the abiogenic magnetite had a smaller particle size than the biogenic material. However, the presence of residual organic material (from the bacteria) could also have been a contributing factor to the higher SSA.

The extent and thickness of the magnetite coatings onto the sand grains were investigated by light microscopy of the entire grains (Fig. 1) and thin sections (Fig. 2). Lower magnification images for the entire grains and thin sections are shown in the SI (Fig. S1 and S2), along with measured coating-layer thicknesses. The distribution of measured layer thicknesses, for each substrate, are presented in Fig. 3. In general, the measured layer thicknesses for the abiogenically coated sand exhibited a roughly normal distribution, whereas all other treatments exhibited much larger variability.

The clean (uncoated) sand did not show any measurable iron concentration or attraction to a bar magnet (Table 1), suggesting that acid and aqua regia washing procedure successfully removed any potential iron impurities. Microscopy images confirmed these results, where uncoated sand grains appeared characteristically white and mostly translucent (Fig. 1g and h). The coarse sand (Ø: 0.4 – 0.8 mm) had a more spherical shape in comparison to the fine sand (Ø: 0.1 – 0.5 mm). No layer or coating was visible on the edges of the pure sand grains as indicated by thin sections (Fig. 2g and h).

The highest amount of iron coating was achieved by the FH coating for both grain sizes which was used as a starting material for the coating Bio-Coarse and Bio-Fine sands with magnetite. The FH coating yielded the largest increase in SSA for the fine sand, which was 35 times higher than for its uncoated precursor. The total Fe and SSA values are comparable with literature data although they are higher (Flores-Ramírez et al., 2016). This might be due to the direct precipitation of FH onto the sand grains instead of just mixing a FH solution with sand. The FH coating on fine sand grains was heterogeneously distributed with some grains completely coated whilst others had almost no coating (Fig. 1a). Additionally, cracks in the surface ferrihydrite layer are clearly visible which might indicate an unstable coating. The instability could also be seen in the background where single unattached iron "flakes" were located next to the grains. This might be caused by abrasion during the handling of the material. The dark red colour potentially indicates a relatively thick iron layer on the grains, confirmed by thin sections. From the thin sections, an iron layer thickness between 2.0 µm–20.2 µm (Fig. 3 and S2) was recorded for the FH coating. The FH coarse sand coating exhibited a more homogenous distribution (Fig. 3a and b) of the iron layer with just few uncoated areas (Fig. 1b). In contrast to the fine sand, the main coating of the coarse sand has a bright red colour with a smaller thickness (Average: 5.6 µm, Fig. 3b), although small dark "flakes" are also obvious, evident from the thin section in Fig. 2b.

After the transformation of the FH coating to biogenic magnetite by *G. sulfurreducens*, the Fe(II)/Fe(III) ratio of Bio-Coarse increased from 0 to ~0.5 (stoichiometric magnetite) with a corresponding colour change from red to black, and a clear development of magnetization (Table 1) (Cornell and Schwertmann, 2003). A loss of total Fe was detected during the coating transformation from FH to magnetite, likely due to loss of loosely associated FH "flakes", visible in the light micrographs (see Figs. 1 and 2). The biogenic transformation of ferrihydrite to magnetite decreased the SSA of the coated fine sand by ~3.6 times. The Bio-Fine sand showed the lowest Fe(II)/Fe(III) ratio (0.23) of all the synthesized magnetite materials. This is potentially related to the presence of thick FH "flakes" coated onto the fine sand. These "flakes" are an aggregation of FH particles which can yield lower accessible surface sites for bacteria and, thus, a lower FH-reduction rate, as described in Piepenbrock et al. (2011). Evidence for incomplete reduction can also be observed in the light micrographs in which several spots on the sand grains remained red (Fig. 1c), indicating the presence of residual FH. In contrast, the measured Fe(II)/Fe(III) ratio for Bio-Coarse, 0.48, was close to stoichiometric magnetite. A loss of Fe(tot) of about 50 % was measured indicating loss of loosely attached FH coating. Thin sections indicated that the coated layers were on average 4.9 µm and 7.0 µm for the Bio-Coarse and Bio-Fine treatments, respectively (Fig. 2c and d, Fig. 3c and d). The majority of the grains in the biogenic coating treatment were coated with a black, greyish layer. However, some small red spots were visible. The transformation to Bio-Coarse led to a 3-fold decrease of SSA in comparison to the FH-Coarse sand precursor material.

The second approach to coat magnetite onto sand grains was through pure chemical (abiotic) precipitation. The abiogenic fine sand (Abio-Fine) had about half of the total iron in comparison to the Bio-Fine sand (0.10 mmol Fe/g_{sand} and 0.19 mmol Fe/g_{sand} respectively), but an Fe(II)/Fe(III) ratio of 0.49, close to stoichiometric magnetite. This abiogenic coating approach showed the lowest increase of SSA to 1.12 m^2/g which is at least 6.6 times the SSA of the pure fine sand (0.17 m^2/g). However, the coating was black and homogeneously distributed with relatively few transparent spots (Fig. 1e). The iron layers formed via this synthesis approach were on average 2.7 µm (2.6 times thinner than for the Bio-Fine treatment) without any indications of "flaking" as observed for Bio-Fine (Fig. 2e and Fig. 3e). Similar properties were achieved for the abiogenic coarse sand (Abio-Coarse). The SSA increased about ~10 times with respect to the starting material (in this case clean sand), and had a comparable Fe(II)/Fe(III) ratio as Abio-Fine (0.49). The total amount of iron was comparable to Bio-Coarse and FH-Fine. The coating was homogeneously distributed over the entire sand grains (Fig. 1f). The grains were covered with a dark black color with almost no evidence of uncoated spots. There was also no obvious "flake" formation. The iron coating appears homogeneously distributed with the same average layer thickness of 2.7 µm as for the Abio-Fine, distributed over each grain (Fig. 2f, Fig. S2, Fig. 3f).

Overall, the different types of approaches used to synthesize pure or coated sand grains led to the formation of magnetite with an Fe(II)/Fe

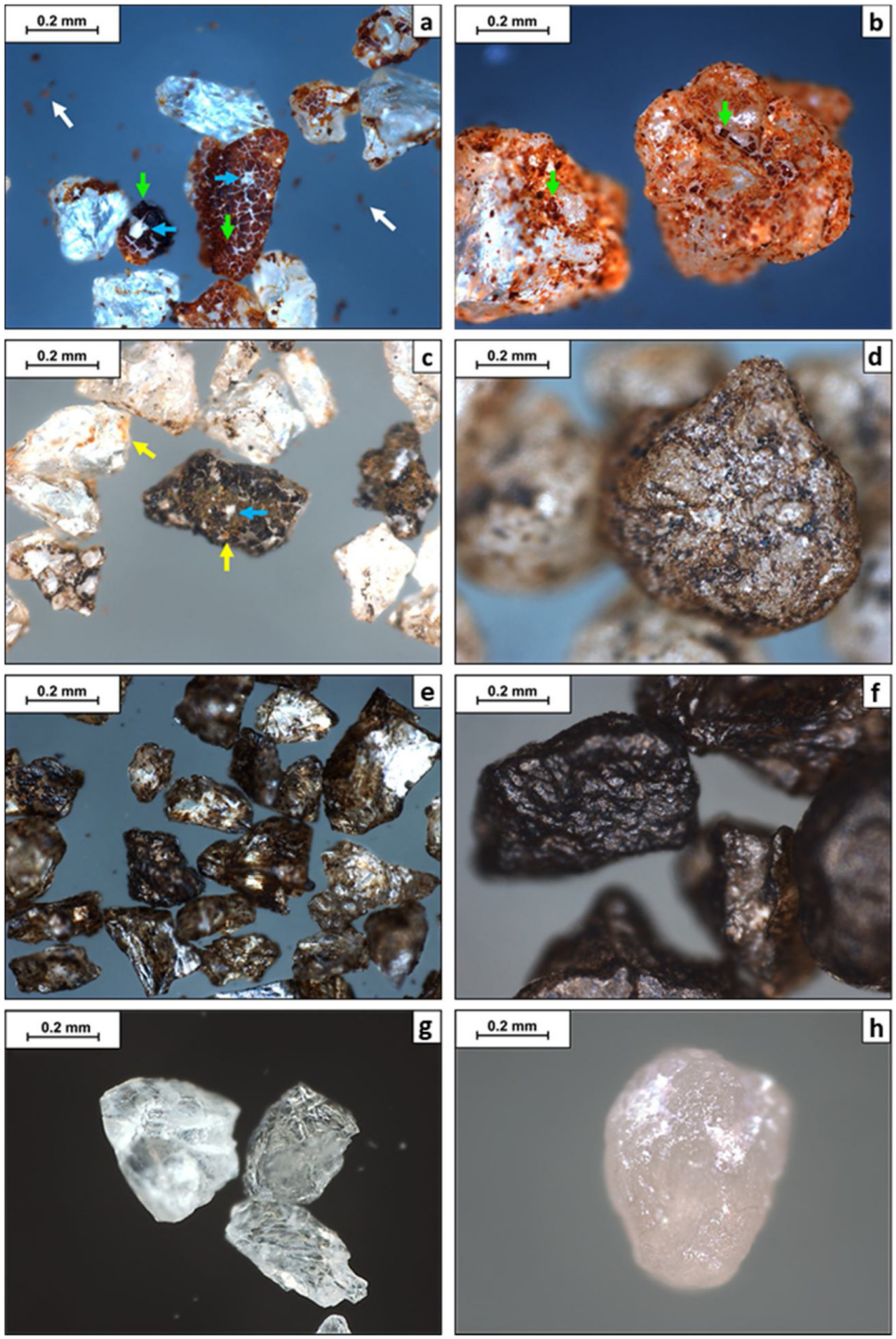

Fig. 1. Light micrographs of, a) ferrihydrite coated fine sand (FH-Fine), b) ferrihydrite coated coarse sand (FH-Coarse), c) biogenic magnetite coated fine sand (Bio-Fine), d) biogenic magnetite coated coarse sand (Bio-Coarse), e) abiogenic magnetite coated fine sand (Abio-Fine), f) abiogenic magnetite coated coarse sand (Abio-Coarse), g) Pure-Fine sand and h) Pure-Coarse sand. Blue arrows indicate cracks and spots where the coating was lost. Green arrows indicate thick FH coatings. White arrows indicate lost FH coatings. Yellow arrows indicate incomplete reduction of FH.

(III) ratio close to stoichiometric magnetite except in the case of Bio-Fine sand. Compared to other synthesis methods (Kango and Kumar, 2016; Wang et al., 2015), all materials presented here could be prepared in a short timeframe, without the use of high temperature or pressure, and with a high coating efficiency (Hanna, 2007). Especially the abiogenic approach can be realized in approximately one day. Additionally, a thinner and visually more homogeneously distributed coating could be achieved by the abiogenic coating procedure, in comparison to the biogenic magnetite coating (Fig. 1–3). The efficiency of the biogenic approach largely depends on the efficiency of the precursor FH coating step. The most homogeneous biogenic coating was achieved for the coarse sand treatment (Fig. 1a and b and Fig. 3a and b). Conversely, the abiogenic approach yielded a high coating efficiency, independent of the sand-grain size (Fig. 3e and f). The simplicity of the approaches presented here, provides a relatively straight forward pathway to upscale the amount of produced material, and, in particular, highlights the simplicity and efficacy of the abiogenic coating approach.

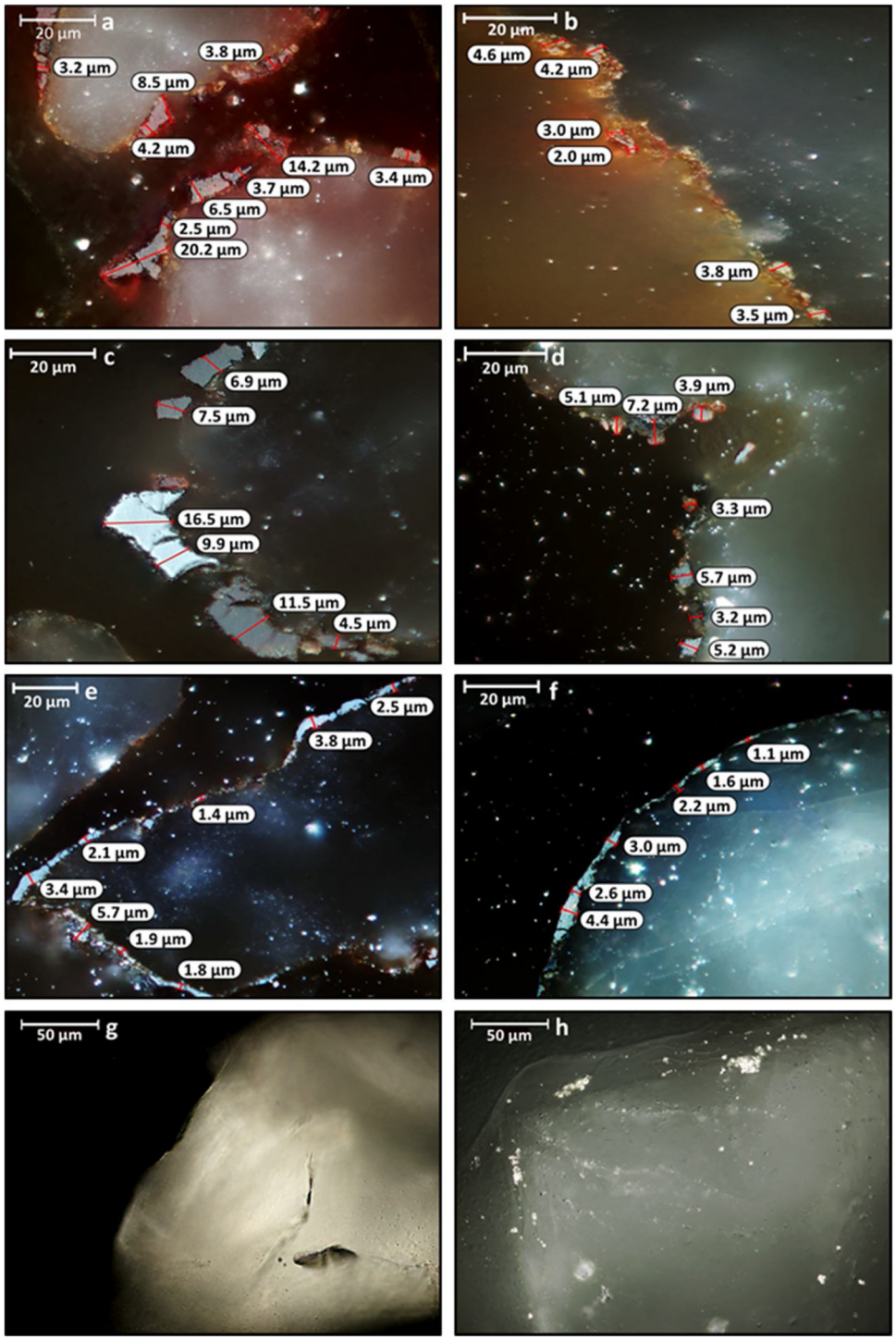

Fig. 2. Light micrographs of thin sections prepared for a) ferrihydrite coated fine sand (FH-Fine), b) ferrihydrite coated coarse sand (FH-Coarse), c) biogenic magnetite coated fine sand (Bio-Fine), d) biogenic magnetite coated coarse sand (Bio-Coarse), e) abiogenic magnetite coated fine sand (Abio-Fine), f) abiogenic magnetite coated coarse sand (Abio-Coarse), g) Pure-Fine sand and h) Pure-Coarse sand. Red bars indicate layer thickness measurements.

3.2. Removal of Cr from solution by magnetite nanoparticles and magnetite-coated sand

Equilibrium aqueous (c_w) and sorbed (c_s) concentration measurements along with fitted Langmuir isotherms are presented in Fig. 4, for each nanoparticle type and magnetite coating treatment. The equilibrium concentration in solution was measured at the end of each sorption experiment (Table S1), and c_s was calculated from the difference between the total starting amount of Cr and c_w. Sorbed concentration results on pure coarse and fine sands are plotted alongside the magnetite coated treatments as a control (Fig. 4c-f), and highlight that no significant sorption of Cr occurred onto the uncoated starting materials.

The reaction between Cr(VI) and magnetite is a combination of a redox reaction and adsorption which involves the reduction of Cr(VI) to Cr(III) and the incorporation of Cr(III) into the octahedral sites of the magnetite structure. Thus, our measured c_s inherently quantifies an integrated contribution of true sorption and the reduction and

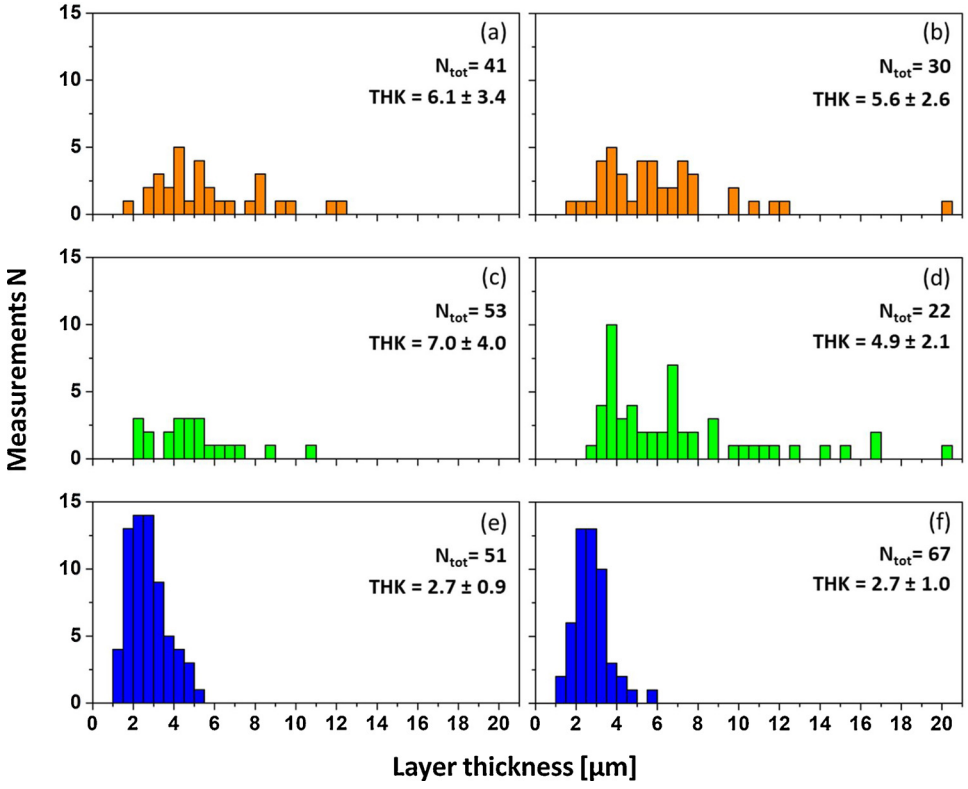

Fig. 3. Measured distributions (for N_{tot} samples) of iron-coating layer thickness for a) ferrihydrite coated fine sand (FH-Fine), b) ferrihydrite coated coarse sand (FH-Coarse), c) biogenic magnetite coated fine sand (Bio-Fine), d) biogenic magnetite coated coarse sand (Bio-Coarse), e) abiogenic magnetite coated fine sand (Abio-Fine) and f) abiogenic magnetite coated coarse sand (Abio-Coarse). THK represents the average layer thickness and standard deviation of the different materials.

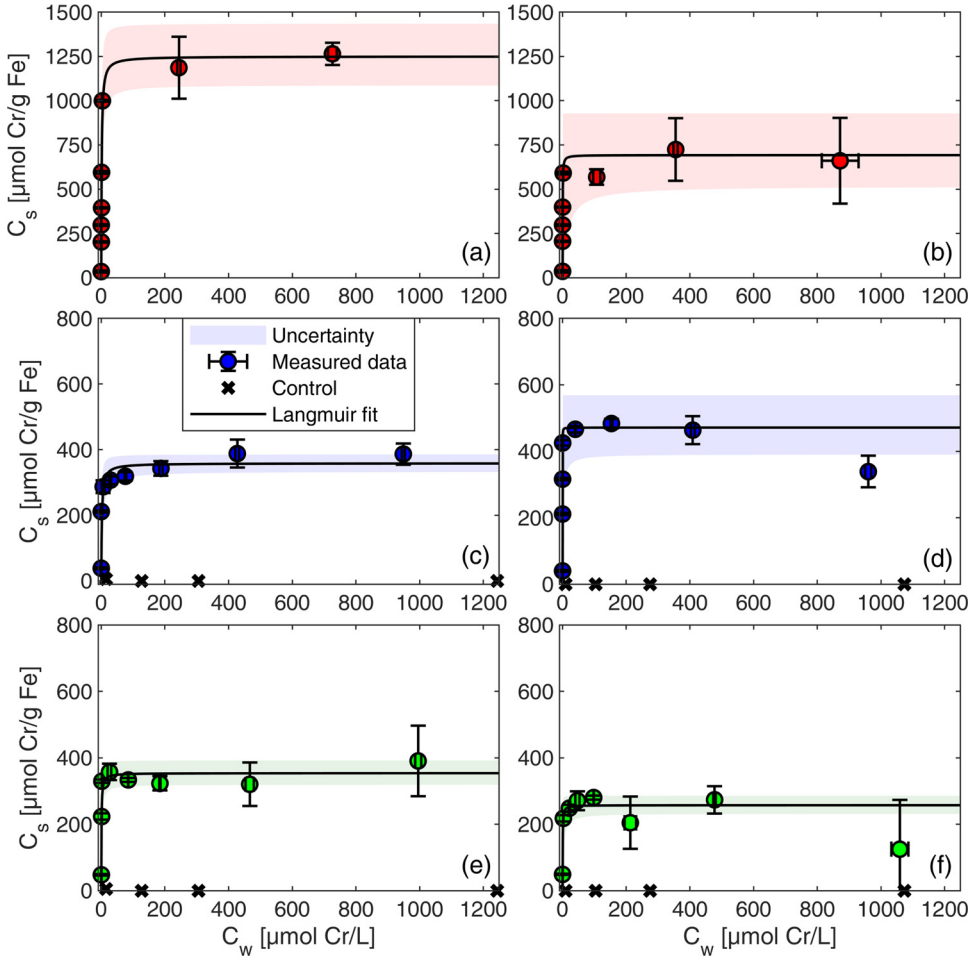

Fig. 4. Measured and fitted Langmuir isotherm results for the various sorption experiments, for a range of Cr(VI) concentrations between 10 – 1000 µM for a) biogenic magnetite nanoparticles (Bio-NP), b) abiogenic magnetite nanoparticles (Abio-NP), c) abiogenic magnetite coated coarse sand (Abio-Coarse), d) abiogenic magnetite coated fine sand (Abio-Fine), e) biogenic magnetite coated coarse sand (Bio-Coarse) and f) biogenic magnetite coated fine sand (Bio-Fine). The concentrations of sorbed and aqueous Cr, c_s and c_w, respectively, are shown (colored circles). The shaded area surrounding the fitted curves represents an estimate of the relative uncertainty. Black crosses represent the control measurements either for pure coarse sand (c and e) or pure fine sand (d and f).

incorporation of Cr(III) into the magnetite structure. Our experimental design does not, however, allow us to decouple these processes from one another. Nevertheless, they both constitute a removal of Cr from solution and a partitioning onto a solid bound form, either as a surface complex or integration into the octahedral structure. Because our data suggest that both of these processes result in an integrated removal of Cr that reaches a maximum, we assume that a saturation-type mechanistic model, the Langmuir model, can adequately quantify the maximum equilibrium binding capacity and thus removal efficiency of Cr onto our synthesized magnetite materials. Further, the Langmuir model as a relevant model for magnetite mediated Cr removal has been widely applied in previous studies (Ren et al., 2017; Yuan et al., 2009). The fitted Langmuir isotherms along with their uncertainty bounds are presented in Fig. 4. Uncertainty bounds are based on the relative uncertainty range of the fitted maximum sorption capacity Q_{max} and the half-saturation concentration K_{ads} (Note: Small K_{ads} values indicate a high affinity to the binding sites). A summary of calibrated parameter values is included in Table S3.

The biogenic and abiogenic nanoparticles showed the highest potential removal of Cr(VI), from solution. Bio-NP had a Q_{max} of 1250 µmol Cr/g Fe which was higher than the Abio-NP with a Q_{max} of 693 µmol Cr/g Fe. For Bio-NP, a Cr(VI) concentration up to 1000 µmol Cr/g Fe could be removed almost completely after 24 h whereas Abio-NP only showed complete removal up to 600 µmol Cr/g Fe. A similar efficiency as for the Abio-NP material was determined with the Abio-Fine sand. Here, a Q_{max} of 471 µmol Cr/g Fe was achieved. The highest concentration for a complete removal with Abio-Fine was up to ~425 µmol Cr/g Fe. Bio-Coarse and Abio-Coarse sand showed similar removal efficacy to each other with respect to hexavalent Cr removal with a Q_{max} of 354 and 358 µmol Cr/g Fe respectively. Both materials removed up to ~300 µmol Cr/g Fe Cr completely from solution. Bio-Fine sand exhibited the lowest sorption capacity, a Q_{max} of 257 µmol Cr/g Fe. Additionally, only up to 200 µmol Cr/g Fe could be sorbed completely. Our fitted Q_{max} values for magnetite coated sands are within the range of previously reported Q_{max} values for magnetite nanoparticles and montmorillonite-supported magnetite nanoparticles (Ren et al., 2017; Yuan et al., 2009). However, the maximum sorption capacity for the biogenic and abiogenic nanoparticles synthesized in this study was 2–3 times higher than those reported previously. Furthermore, our fitted K_{ads} was at least one order of magnitude lower than previously reported (e.g. Ren et al., 2017), suggesting a relatively high affinity of the materials used here to Cr. All fitted K_{ads} values fall within the range of uncertainty values for each case and highlight a similar affinity for Cr for all treatments.

Differences in SSA seem to play a minor role in controlling the Cr-removal capacity of the different materials studied herein. A 64-fold larger SSA was measured for Abio-NP than Abio-Fine, but the removal efficiency of Abio-NP was still similar for Abio-Fine in comparison to Abio-NP. Thus, based on our results the Fe(II)/Fe(III) ratio appears to exert a more important control on the Cr-binding capacity of magnetite than its surface area (for the range of surface areas studies here), in agreement with previous findings (Gorski et al., 2010). Further evidence to support this hypothesis lies in the much higher maximum sorption capacity exhibited by biogenic magnetite nanoparticles than abiogenically synthesized ones. Despite the higher surface area of abiogenic nanoparticles (almost twice as large as biogenic nanoparticles), biogenic particles, with an Fe(II)/Fe(III) ratio of 0.63, could potentially remove 1.8 times more Cr than their abiogenic counterparts based on the calculated Q_{max} values. In summary, both biogenically and abiogenically coated sands strongly adsorbed Cr, effectively removing it from solution. Differences in the sorption capacity of the materials did not reflect a strong influence of whether the magnetite was biologically produced or not.

4. Conclusions

Here we have synthesized biogenic and abiogenic magnetite nanoparticles as well as precipitated biogenic or abiogenic magnetite coatings onto fine and coarse sand grains. The synthesized materials exhibited the maximum sorption capacity towards hexavalent chromium in the following order: Bio-NP > Abio-NP > Abio-Fine sand > Abio-Coarse sand > Bio-Coarse sand > Bio-Fine sand. In general, Bio-NP exhibited the highest Cr removal efficiency as expected, and Bio-Fine sand the lowest, based on the total amount of iron. Although, the magnetite nanoparticles showed the highest reactivity, Abio-Fine sand still exhibited a high capacity to remove Cr(VI) even comparable with magnetite nanoparticles reported in the literature. The effect of SSA of the material was observed to be relatively minor in comparison to the Fe(II)/Fe(III) ratio of magnetite with respect to removal efficiency. Therefore, the disadvantages like the transport of nanoparticles, the agglomeration and potential pressure drops in column filters as well as the need to apply expensive external electromagnetic fields to separate magnetite nanoparticles from solution can be overcome. By using magnetite sand coatings magnetite can be fixed in place and still maintain the advantages of using “free” magnetite nanoparticles towards Cr(VI) removal performance. Furthermore, if magnetite nanoparticles are released to the aquatic environment, they can aggregate and lose their high surface area and high reactivity towards Cr. This can also be overcome by coating sand with magnetite. Comparing the effort in preparing the different materials with the performance towards Cr (VI) removal, abiogenically coated sand is the better choice in comparison to the biogenically coated sand. With our method, the synthesis of abiogenic magnetite coated sand can be produced in approximately one day and easily upscaled to produce a larger amount of this material. Nevertheless, a further improvement of the abiogenic coated sand could be achieved by enhancing the stoichiometry of the magnetite through the use of either Fe(III)-reducing or Fe(II)-oxidizing bacteria.

CRediT authorship contribution statement

Julian Sorwat: Conceptualization, Methodology, Investigation, Writing - original draft, Visualization. **Adrian Mellage:** Formal analysis, Writing - original draft, Visualization. **Andreas Kappler:** Conceptualization, Supervision, Writing - original draft. **James M. Byrne:** Conceptualization, Supervision, Visualization, Writing - original draft.

Declaration of Competing Interests

The authors declare that they have no known competing financial interests or personal relationships that could have appeared to influence the work reported in this paper

Acknowledgements

This work was supported by funding awarded to J Byrne as part of the Baden Wuerttemberg RiSC program, and Deutsche Forschungsgemeinschaft (BY 82/2-1). Many thanks to Per Jeisecke for embedding and processing our sand samples. Further, we want to thank Dr. Bertrand Ligouis for access and help with the Leica DMRX optical microscope and his support polishing our embedded grain samples. Many thanks also to Sara Roci who contributed significantly to this work.

Appendix A. Supplementary data

Supplementary material related to this article can be found, in the online version, at doi:https://doi.org/10.1016/j.jhazmat.2020.123139.

References

Ali, S.W., Mirza, M.L., Bhatti, T.M., 2015. Removal of Cr(VI) using iron nanoparticles supported on porous cation-exchange resin. Hydrometallurgy 157, 82–89.

Avudainayagam, S., et al., 2003. Chemistry of chromium in soils with emphasis on tannery waste sites. Rev. Environ. Contam. Toxicol. 178, 53–91.

Barnhart, J., 1997. Occurrences, uses, and properties of chromium. Regul. Toxicol. Pharmacol. 26, S3–S7 0273-2300 (Print).

Berry, C.C., et al., 2004. Cell response to dextran-derivatised iron oxide nanoparticles post internalisation. Biomaterials 25 (23), 5405–5413.

Brezonik, P.L., Arnold, W.A., 2012. Water chemistry: fifty years of change and progress. Environ. Sci. Technol. 46 (11), 5650–5657.

Brown, D.M., et al., 2001. Size-dependent proinflammatory effects of ultrafine polystyrene particles: a role for surface area and oxidative stress in the enhanced activity of Ultrafines. Toxicol. Appl. Pharmacol. 175 (3), 191–199.

Byrne, J.M., et al., 2011. Control of nanoparticle size, reactivity and magnetic properties during the bioproduction of magnetite by Geobacter sulfurreducens. Nanotechnology 22, 455709.

Byrne, J.M., et al., 2015. Scale-up of the production of highly reactive biogenic magnetite nanoparticles using Geobacter sulfurreducens. J. R. Soc. Interface 12.

Chahbani, M.H., Tondeur, D., 2001. Pressure drop in fixed-bed adsorbers. Chem. Eng. J. 81, 23–34.

Cornell, R.M., Schwertmann, U., 2003. The Iron Oxides: Structure, Properties, Reactions, Occurrences and Uses. Wiley-VCH Verlag GmbH & Co. KGaA.

Crean, D.E., et al., 2012. Engineering biogenic magnetite for sustained Cr(VI) remediation in flow-through systems. Environ. Sci. Technol. 46 (6), 3352–3359.

Cutting, R., et al., 2010. Optimizing Cr(VI) and Tc(VII) remediation through nanoscale biomineral engineering. Environ. Sci. Technol. 44, 2577–2584.

Duruibe, J., Ogwuegbu, M.O.C., Egwurugwu, J., 2007. Heavy metal pollution and human biotoxic effects. Int. J. Phys. Sci. 2, 112–118.

Environmental Protection Agency, Retrieved July 19, from https://www.epa.gov/dwstandardsregulations/chromium-drinking-water. 2019.

Fendorf, S.E., Li, G., 1996. Kinetics of chromate reduction by ferrous Iron. Environ. Sci. Technol. 30 (5), 1614–1617.

Flores-Ramírez, E., Dominik, P., Kaupenjohann, M., 2016. Novel ferrihydrite sand coating process as a first step for designed technosols. J. Soils Sediments 18, 3349–3359.

García, A., et al., 2011. Acute toxicity of cerium oxide, titanium oxide and iron oxide nanoparticles using standardized tests. Desalination 269 (1), 136–141.

Gorski, C.A., et al., 2010. Redox behavior of magnetite: implications for contaminant reduction. Environ. Sci. Technol. 44 (1), 55–60.

Hanna, K., 2007. Adsorption of aromatic carboxylate compounds on the surface of synthesized iron oxide-coated sands. Appl. Geochem. 22 (9), 2045–2053.

Harijan, D.K.L., Chandra, V., 2016. Environment friendly synthesis of magnetite–-graphene composite for adsorption of toxic chromium (VI) ions from drinking water. Environ. Prog. Sustain. Energy 35 (3), 700–705.

Kango, S., Kumar, R., 2016. Magnetite nanoparticles coated sand for arsenic removal from drinking water. Environ. Earth Sci. 75 (5), 381.

Kleinert, S., et al., 2011. Biogenic Fe(III) minerals lower the efficiency of iron-mineral-Based commercial filter systems for arsenic removal. Environ. Sci. Technol. 45 (17), 7533–7541.

LeBel, C.P., Ischiropoulos, H., Bondy, S.C., 1992. Evaluation of the probe 2',7'-dichlorofluorescin as an indicator of reactive oxygen species formation and oxidative stress. Chem. Res. Toxicol. 5, 227–231 0893-228X (Print).

Li, H., et al., 2009. Effects of waterborne nano-iron on medaka (Oryzias latipes): antioxidant enzymatic activity, lipid peroxidation and histopathology. Ecotoxicol. Environ. Saf. 72 (3), 684–692.

Limbach, L.K., et al., 2008. Removal of oxide nanoparticles in a model wastewater treatment plant: influence of agglomeration and surfactants on clearing efficiency. Environ. Sci. Technol. 42 (15), 5828–5833.

Lovley, D.R., Phillips, E.J., 1986. Availability of ferric iron for microbial reduction in bottom sediments of the freshwater tidal potomac river. Appl. Environ. Microbiol. 52 (4), 751–757.

Maher, B.A., et al., 2016. Magnetite pollution nanoparticles in the human brain. Proc. Natl. Acad. Sci. U.S.A. 113 (39), 10797–10801.

Meranger, J.C., Subramanian, K.S., Chalifoux, C., 1979. A national survey for cadmium, chromium, copper, lead, zinc, calcium, and magnesium in Canadian drinking water supplies. Environ. Sci. Technol. 13 (6), 707–711.

Micera, G., Dessì, A., 1988. Chromium adsorption by plant roots and formation of long-lived Cr(V) species: an ecological hazard? J. Inorg. Biochem. 34 (3), 157–166.

Nriagu, J.O., Nieboer, E., 1988. Chromium in Natural and Human Environments. John Wiley & Sons.

Panyam, J., Labhasetwar, V., 2003. Biodegradable nanoparticles for drug and gene delivery to cells and tissue. Adv. Drug Deliv. Rev. 55 (3), 329–347.

Pearce, C.I., et al., 2012. Synthesis and properties of titanomagnetite (Fe3−xTixO4) nanoparticles: a tunable solid-state Fe(II/III) redox system. J. Colloid Interface Sci. 387 (1), 24–38.

Peterson, P.J., 1975. In: In Proceedings of the International Conference on Heavy Metals in the Environment. Ed. T C Hutchinson. 2, 39, University of Toronto, Canada.

Petosa, A.R., et al., 2010. Aggregation and deposition of engineered nanomaterials in aquatic environments: role of physicochemical interactions. Environ. Sci. Technol. 44 (17), 6532–6549.

Phenrat, T., et al., 2009. Particle size distribution, concentration, and magnetic attraction affect transport of polymer-modified Fe0 nanoparticles in sand columns. Environ. Sci. Technol. 43 (13), 5079–5085.

Piepenbrock, A., et al., 2011. Dependence of microbial magnetite formation on humic substance and ferrihydrite concentrations. Geochim. Cosmochim. Acta 75 (22), 6844–6858.

Ren, G., et al., 2017. Chromium (VI) adsorption from wastewater using porous magnetite nanoparticles prepared from titanium residue by a novel solid-phase reduction method. Sci. Total Environ. 607–608, 900–910.

Salunkhe, P.B., Dhakephalkar, P., Paknikar, K., 1998. Bioremediation of hexavalent chromium in soil microcosms. Biotechnol. Lett. 20, 749.

Stookey, L.L., 1970. Ferrozine—a new spectrophotometric reagent for iron. Anal. Chem. 42 (7), 779–781.

Sundman, A., et al., 2020. Effect of Fe-metabolizing bacteria and humic substances on magnetite nanoparticle reactivity towards arsenic and chromium. J. Hazard. Mater. 384, 121450.

Terry, N., Banuelos, G.S., 1999. Phytoremediation of Contaminated Soil and Water. CRC Press, Boca Raton.

Tratnyek, P.G., Johnson, R.L., 2006. Nanotechnologies for environmental cleanup. Nano Today 1 (2), 44–48.

Umweltbundesamt, 2012. Potentielle Schädlichkeit Von Chrom Im Trinkwasser Einordnung Der Epidemiologischen Befunde Zum Krebsrisiko Nach Exposition Von Populationen Gegenüber Chrom(VI) Im Trinkwasser Und Vorschlag Zur Ableitung Einer Expositions-Risikobeziehung 2012 Bericht zum Sondervorhaben des Umweltbundesamtes FKZ 363.

US Environmental Protection Agency, 1987. Office of Drinking Water. Health Advisory—chromium. Washington, DC. .

Verbinnen, B., et al., 2013. Simultaneous removal of molybdenum, Antimony and selenium oxyanions from wastewater by adsorption on supported magnetite. Waste Biomass Valorization 4, 635–645.

Wang, Y., et al., 2015. Arsenite and arsenate leaching and retention on iron (hydr)oxide-coated sand column. J. Soils Sediments 16, 486–496.

World Health Organization, 1996. Guidelines for Drinking-Water Quality. Health Criteria and Other Supporting Information 2.

World Health Organization, 2017. Incorporating the first addendum. Guidelines for Drinking-Water Quality, fourth edition. .

Yao, Z., et al., 2015. Positively charged membrane for removing low concentration Cr(VI) in ultrafiltration process. J. Water Process. Eng. 8, 99–107.

Yuan, P., et al., 2009. Montmorillonite-supported magnetite nanoparticles for the removal of hexavalent chromium [Cr(VI)] from aqueous solutions. J. Hazard. Mater. 166 (2), 821–829.